Fabrication and Analysis of Gecko-Inspired Hierarchical Polymer Nanosetae

Audrey Yoke Yee Ho,[†,‡] Lip Pin Yeo,[‡,§] Yee Cheong Lam,[‡,§] and Isabel Rodríguez[†,*]

[†]Institute of Materials Research & Engineering, A*STAR (Agency for Science, Technology and Research), 3 Research Link, Singapore 117602, [‡]School of Mechanical & Aerospace Engineering, Manufacturing Division, Nanyang Technological University, Nanyang Avenue, Singapore 639798, and [§]Singapore—MIT Alliance, Manufacturing Systems and Technology Program, Nanyang Technological University, Singapore 637460

ABSTRACT A gecko's superb ability to adhere to surfaces is widely credited to the large attachment area of the hierarchical and fibrillar structure on its feet. The combination of these two features provides the necessary compliance for the gecko toe-pad to effectively engage a high percentage of the spatulae at each step to any kind of surface topography. With the use of multi-tiered porous anodic alumina template and capillary force assisted nanoimprinting, we have successfully fabricated a gecko-inspired hierarchical topography of branched nanopillars on a stiff polymer. We also demonstrated that the hierarchical topography improved the shear adhesion force over a topography of linear structures by 150%. A systematic analysis to understand the phenomenon was performed. It was determined that the effective stiffness of the hierarchical branched structure was lower than that of the linear structure. The reduction in effective stiffness favored a more efficient bending of the branched topography and a better compliance to a test surface, hence resulting in a higher area of residual deformation. As the area of residual deformation increased, the shear adhesion force emulated. The branched pillar topography also showed a marked increase in hydrophobicity, which is an essential property in the practical applications of these structures for good self-cleaning in dry adhesion conditions.

KEYWORDS: gecko-inspired adhesion · dry adhesion · branched porous anodic alumina · hierarchical nanostructures

A gecko's superb ability to adhere to surfaces is widely credited to the large attachment area of approximately 220 mm^2 of *hierarchical* and *fibrillar* structures on its feet.[1] The combination of these two features provides the necessary compliance to the gecko toe-pad to effectively engage a high percentage of the spatulae, at each step, to any kind of surface topography.[2] The fibrils begin from rows of lamellae. Each row consists of thousands of primary setal stalks known as setae.[3] Autumn *et al.*[4] estimated that there are 14 400 setae/mm^2. Each seta is approximately 30−130 μm in length and 5−10 μm in diameter consisting of three levels.[5] The secondary seta is about 20−30 μm in length and 1−2 μm in diameter. At the end of each secondary seta, 100−1000 spatulae with a diameter of 100−200 nm form the points of contact with a surface. The tips of the spatulae are approximately 200−300 nm in width,[5] 500 nm in length, and 10 nm in thickness.[6]

Cumulative van der Waals interactions have been attributed to be the main adhesive mechanism[7] achieved through contact splitting of setae.[8] However, it is the hierarchical topography that allows for an effective compliance to a surface by decreasing the stiffness of each level of seta[9] with the spatula maintaining sufficient mechanical stability. To have the same compliance to a surface without the hierarchical structure, linear β-keratin setae would have to have a length of 160 μm (aspect ratio of 100−160). At this aspect ratio, the mechanical stability of the pillars would be insufficient, resulting in clumping and collapse of the pillars. Clumping of the setae is undesirable as this would reduce the contact points.[10] In addition, these clumped or bunched pillars would have higher stiffness and thus lower compliance.[10,11]

Theoretically, Gao *et al.*[12] have shown that, by having a hierarchical structure, the theoretical van der Waals adhesion strength between surfaces can be reached. Numerically, Kim *et al.*[13] showed that a hierarchical setae structure provides geckos with the adaptability to have large effective area of contact with rough surfaces. He later showed that the equivalent stiffness of a three-level hierarchical structure is approximately 40% lower than a one-level linear structure. Such reduction in stiffness resulted in more than 100% enhancement in adhesion energy.[14]

The focus of fabrication of gecko-mimetic structures has shifted to obtain hierarchical structures through various methods[15−18] to replicate as close as possible the

* Address correspondence to i-rodriguez@imre.a-star.edu.sg.

Received for review October 15, 2010 and accepted February 14, 2011.

Published online February 28, 2011
10.1021/nn103191q

topographic features found in geckos and possibly satisfying all seven requisites for dry adhesion proposed by Autumn *et al.*[19] Greiner *et al.*[16] fabricated hierarchical pillars in PDMS. The base pillars were 50 μm in diameter and 200 μm in length. The top round-ended pillars were 10 μm in diameter with aspect ratios ranging from 0.5 to 2. Contrary to what was expected, the pull-off test showed an order of magnitude lower pull-off force for these hierarchical structures. This was attributed to the lower packing density of the hierarchical structure when compared to a linear structure (aspect ratio of 1). Jeong *et al.*[18] had similar observations. They fabricated a hierarchical structure with base pillars of 5 μm diameter and height of 25 μm with slanted top pillars (with flat ends) of 600 nm in diameter and 3 μm in height. The shear adhesion of this topography was tested against a flat surface and compared with topography of a slanted linear structure with the dimensions of the top pillars. Significantly lower shear adhesion was obtained for the hierarchical structure ($\approx$9 N/cm^2) as opposed to the slanted linear structure ($\approx$21 N/cm^2). In contrast, Murphy *et al.*[17] reported a two-level hierarchical structure which has higher adhesion when compared to the linear structures. The reason cited was that the hierarchical structure enabled the reduction of the effective modulus of the material, thus leading to an increase in the contact area experienced by the hemispherical indenter. The materials reported in these investigations were typically soft polymers (elastic modulus of 3−19.8 MPa). It was only Kustandi *et al.*[15] who reported the use of a stiff polymer (PMMA) in his effort to fabricate hierarchical structures by sequentially using two porous alumina templates. However, clumping due to the densely packed pillars was observed on the fabricated films. As a result, the adhesion force of these structures could not be determined accurately. These studies, with several structural variations, however, were inconclusive in proving the advantages of a hierarchical structure. The above-mentioned background serves as a motivation for this present work.

Here, we present an effective method for the fabrication of nanometer ranged hierarchically structured stiff polymer films, using multi-tiered branched porous anodic alumina (PAA) as template.[20] Positive replicates were obtained with capillary force assisted nanoimprinting.[21] With systematic analyses, we also put forth possible explanations for the two distinct phenomena observed: (1) the shear adhesion force of the polymeric structured films increased progressively as the films were repeatedly tested; (2) the hierarchically structured films of branched pillars indeed outperformed the linear pillars in experimental shear adhesion tests. The films with branched pillars showed a 150% higher shear adhesion force than those with linear pillars. Lastly, contact angle measurements on the fabricated topographical films show an increase in hydrophobicity of branched pillars over linear pillars, which imparts the self-cleaning ability of the gecko adhesion system.[19]

The fabrication of hierarchically branched PAA templates has been explained in detail by Ho *et al.*[20] To solely demonstrate the specific effect of a hierarchical structure in improving shear adhesion, a two-level hierarchical structure was used. The overall heights of both the linear and branched structures were fabricated equal (see Figure S1, Supporting Information). This is to avoid ambiguity in the shear adhesion analysis and to ascribe the differences in adhesion to geometrical differences without having to account for the difference in pillar height. Figure S1a,c (Supporting Information) illustrates the cross section and an SEM image of the multi-tiered branched PAA template, respectively. Figure S1b,d depicts the linear PAA. The coding for the dimensions of the templates is also given in Figure S1; namely, *D*, diameter of the first-tiered PAA and diameter of the linear PAA; *H*, overall height of the template; *d*, diameter of the second-tiered PAA template; and *h*, height of the second-tiered PAA template.

Positive replicates were obtained using capillary force assisted nanoimprinting.[21] The polymer used was commercial grade Lexan polycarbonate (PC). It is a thermoplastic material with an elastic modulus of 2.19 $\pm$ 0.09 GPa, comparable to the β-keratin of gecko foot hairs.[19] The pillar density obtained was approximately 6.2 $\times$ 10^6 pillars/mm^2, which is in the same order of magnitude as the natural gecko foot hair.[13] The films were demolded by peeling off the PAA template. The main advantage of demolding by peel-off over wet-etching is that the clumping of high aspect ratio pillars observed by other authors[15] is avoided. The schematic process to obtain the positive replicates of multi-tiered branched PAA in PC is provided as Supporting Information Figure S2. The dimensions of the branched pillars fabricated for shear adhesion tests are the following: base pillars of $\pm$20 nm in diameter and 5.5 $\pm$ 0.5 μm in-height and top branch pillars of diameter and height of 90 $\pm$10 nm and 850 $\pm$ 50 nm, respectively. The corresponding linear pillars utilized for comparisons were 280 $\pm$ 20 nm in diameter and 6.5 $\pm$ 0.5 μm in height. Both samples had a residual bulk layer of thickness of $\sim$150 μm. Figure 1a,b shows some of the SEM images of the branched pillars obtained by varying the anodizing conditions used in the fabrication of the PAA template. The base pillars' dimensions in Figure 1a are 280 $\pm$ 20 nm in diameter with height of 2.5 $\pm$ 0.3 μm and top pillars having a diameter and height of 90 $\pm$ 10 nm and 490 $\pm$ 50 nm, respectively. The branched pillars in Figure 1b had base pillars with diameter and height of 280 $\pm$ 20 nm and 6.5 $\pm$ 0.5 μm, respectively, and top pillars with diameter and height of 110 $\pm$ 10 nm and 600 $\pm$ 50 nm, respectively. The 10−15%

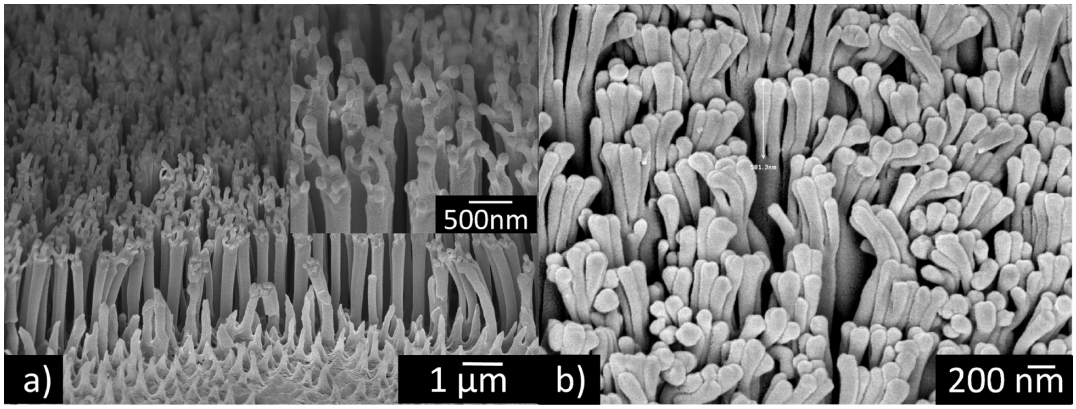

Figure 1. SEM images of fabricated hierarchically branched pillared substrates. (a) Four branches (inset shows magnified view of pillars). The base pillars' dimensions are 280 ± 20 nm in diameter with an aspect ratio of 8−10 and top pillars having a diameter and aspect ratio of 90 ± 10 nm and 5−6, respectively. (b) Five branches. The dimensions of the branched pillars are 280 ± 20 nm and 6.5 ± 0.5 μm for the diameter and height of the base pillars respectively, with top pillars having a diameter and aspect ratio of 110 ± 10 nm and 5−6, respectively.

standard deviation seen in the pillar dimensions are due to the inherent property in the self-assembly processes of the alumina template.[22]

Prior to quantitative shear adhesion force measurements, qualitative tests were first carried out to compare the shear adhesion force of branched pillars *versus* linear pillars. For these tests, the back of the sample was glued to a (1.4 g) metallic disk. The sample was then placed with the pillars facing against a cleaned glass slide. With one end of the glass slide fixed acting as a pivot, the other end was raised. The linear pillars on a metallic disk slid off at 64° tilt, while the branched pillars remained on the glass even at a 90° tilt angle (Figure S3, Supporting Information).

Subsequently, shear adhesion force measurements were carried out to determine quantitatively the performance of the branched pillars and to understand the contribution of the hierarchical structure in adhesion. The shear adhesion measurements were conducted using an Instron 5543 single column universal testing machine (UTM). A load cell was fixed to the machine's crosshead. To translate vertical movement to lateral movement for the shear tests, a ball-bearing Teflon pulley aligned directly under the load cell was used. The sample was then placed with the pillars facing a glass slide. A magnetic disk weighing 45 mN was glued on top of the sample to act as preload. During shear adhesion tests, when the crosshead was extended upward, the sample slid across the glass surface and the corresponding shear force was registered instantaneously. After each measurement, the film with the attached preload was separated from the glass slide. The film (with the pillars facing upward) was then observed under a microscope, and images of the film were captured. This method of contact area observation differs from those reported before, whereby *in situ* video recording of the contact area was employed while shearing[23] or pulling-off[24] of the samples was performed. Here, a more practical approach is used whereby the area of residual deformation is employed to determine the area where pillars have been in contact with the glass test surface. This method was adopted because, consistently, it was seen in the scanning electron micrograph (SEM) images that the pillars after the shear adhesion experiments remained in a deformed state, indicating that the structures experienced plastic deformation and thus incomplete recovery upon load removal. The sample was then returned to be tested with increased preloads. Preloads which consisted of magnetic discs were added on stepped increments of 25 mN, and the same procedure was repeated for each increment. Each test was repeated with three samples. Figure S4a,b (in the Supporting Information) illustrates the schematic as well as the actual test setup, respectively.

For each sample, a control image prior to the shear test was first captured using an optical microscope. As the microscope is limited by its field of view in capturing the entire area of the sample, images were taken in parts and subsequently stitched together before analyzing them with image processing software (ImageJ, version 1.41o). Similar methods of area analyses have been performed by several research groups using different image processing softwares.[23,25] Figure 2a depicts the light contrast of the stitched control image. The stitched image was originally in RGB color and was subsequently quantized to 8-bit grayscale. On the basis of the percentage of pixels of the light contrast of the grayscale image, the percentage of area with light contrast (area fraction) of the control image was determined (see Figure 2c). The light contrast observed, even in the control image, is the contrast from the adhesion layer (layer between the sample and the glass slide) as well as one or two scratches made on top of the sample surface during handling. This was

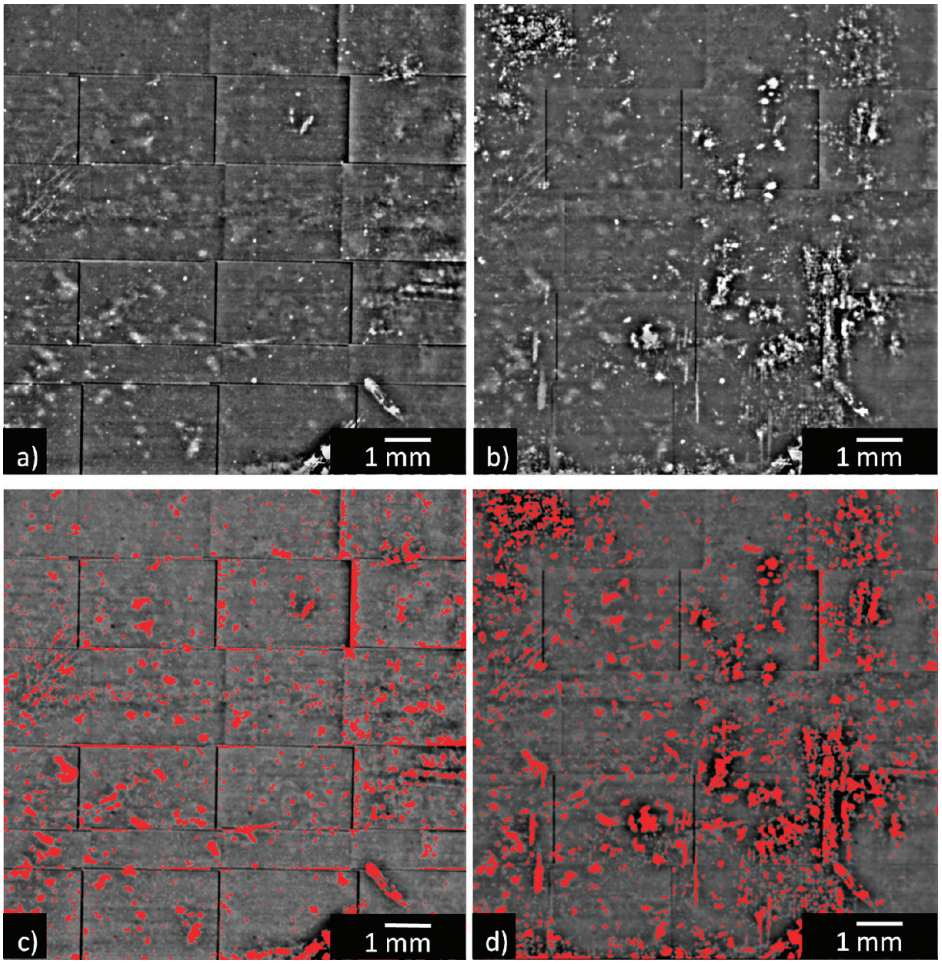

Figure 2. Stitched images of adhesive tapes taken with optical microscope. (a) Control images (prior to shear adhesion test). (b) Images taken after a typical shear force measurement and the removal of preload. The light contrast differences between (a) and (b) correspond to area of residual deformation (effective contact area after the removal of preload) of pillars with the glass slide. Images of (a) and (b) were analyzed using image processing software (ImageJ, v1.41o) and are shown in (c) and (d), respectively.

used as a benchmark for all subsequent images. The same procedure was applied after each shear force measurement and after the removal of the preload. Figure 2 panels b (light contrast image) and d (after area analysis) show the optical images after a typical shear adhesion test. The area of residual deformation was then estimated by subtracting the area fraction of each image after each shear force measurement from the control image. This is based on the assumption that the increase of area fraction was due to the pillars that had been in actual contact with the glass slide increased, which resulted in changes in the light contrast for the contact area, and that some of this deformation did not recover fully after shear even with the removal of the preload. Thus, the observed difference in the light contrast was taken to be the area of residual deformation of the pillars with the glass slide. The ambiguous spots due to focusing difficulty and errors arising caused by stitching of the images have been taken into account by carefully taking three sets of images of the same sample after each test. This is shown through the standard deviations in the graphs.

RESULTS AND DISCUSSION

Figure 3a depicts the shear adhesion forces registered during mechanical testing. An increase of shear adhesion force was observed for all of the substrates when the shear adhesion tests were repeated with the same preload (30 mN). Figure 3a shows that the increase is linear. This observation has previously been reported.[23] While pristine (without pillar structures) PC films did show increase of shear adhesion force during repeated tests, the increase was minimal. The increase in adhesion force for linear pillars was substantial. However, the branched pillars showed a much steeper ascent in consecutive measurements. This increase in adhesion force for the branched pillars as compared to the linear pillars can be assessed by calculating the linear fitted slopes for the shear adhesion plots in consecutive tests. The values obtained are 15.85 $\pm$ 0.44 mN/test for branched pillars *versus* 4.88 $\pm$ 0.23

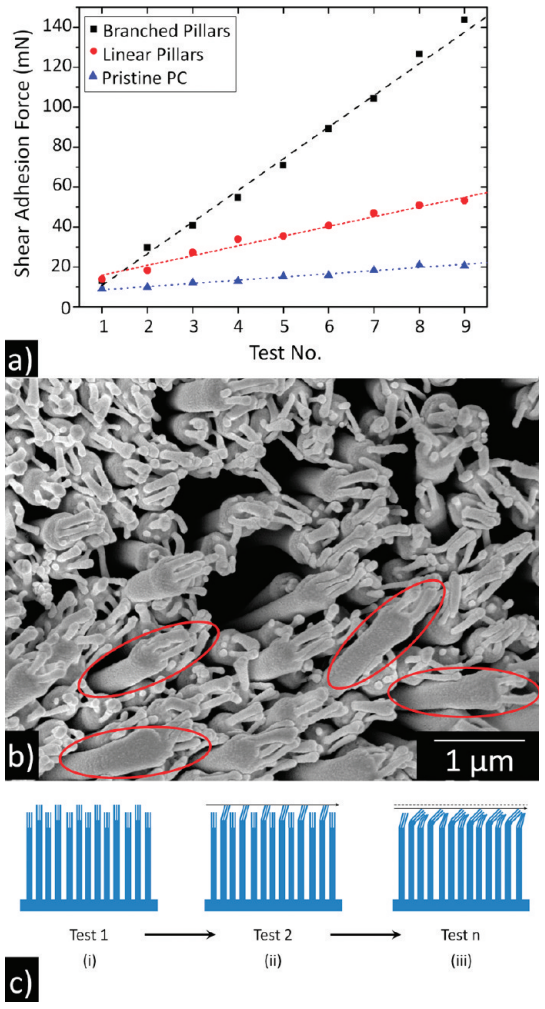

Figure 3. (a) Shear adhesion force of branched, linear pillars and pristine polycarbonate with repeated measurements using same preload of 30 mN. Branched pillars show higher absolute values of shear adhesion force and a marked increase in shear adhesion force in consecutive measurements. Linear fitted slopes are 1.60 ± 0.07 mN/test (R^2 of 0.98) for pristine PC, 15.85 ± 0.44 mN/test (R^2 of 0.99) for branched pillars, and 4.88 ± 0.23 mN/test (R^2 of 0.98) for linear pillars. The slope indicates the increase in adhesive force in each test for the same preload. (b) SEM image showing the conditioning of the branched pillars after a shear adhesion measurement. Circles highlight some of the typical side contacts (outer surface area along the pillar in contact with the shearing surface) of the pillars. (c) Illustration of pillars conditioning for consecutive shear adhesion measurements. (i) Variation in pillars' height means that taller pillars will first be in point contact with the glass surface. (ii) With shearing, pillars deform plastically in shear direction resulting in side contact. (iii) Overall height of pillars is decreased, allowing neighboring pillars to come into contact with glass surface. This increases the area of residual deformation (which could be an indirect indication of effective contact area) and thus results in higher shear adhesion force.

mN/test for linear pillars. An explanation for this observation is that shearing under a preload caused the pillars to deform plastically to the same height during each test resulting in side contact of the pillars (see Figure 3b). The assumption of plastically deformed pillars is supported by the branched pillars remaining in a deformed state, indicating incomplete recovery upon load removal (see Figure 3b). As schematically shown in Figure 3c, due to the inherent non-uniformity of the self-assembled fabrication processes of the PAA template, there was a small variation in pillar height. Thus, we postulate that, during the first shear adhesion experiment, the taller pillars would be the first points of contact with the glass surface. As the pillars were being sheared, the pillars were plastically deformed in the shear direction.[26] As a result, the overall height of the pillared topography was decreased, allowing the shorter pillars to come into contact with the glass surface. In addition, greater number of pillars made side contact to the test surface. Consequently, with this behavior developing during each consecutive test, there was a proportional increase in the area of residual deformation, resulting in higher shear adhesion force in the subsequent shear test. This observation further demonstrates that the pillars were not completely recovered after each test. As such, the area of residual deformation could be used as an indirect indication of the effective area of contact. Theoretically, this increase would persist until all of the pillars came into full contact with the glass slide. However, as the samples were not completely flat and due to the stiff residual bulk polymer substrate (~150 μm thick), full contact of all pillars could not be realized.

Shear adhesion force measurements of substrates with branched and linear pillars at different preloads (from Instron UTM) are shown in Figure 4a. The maximum shear adhesion force, which can be considered as the static friction force just before the substrate starts to slide on the glass surface, was used in the plotting of the graphs. For all preloads higher than 65 mN, the branched pillars exhibited higher shear adhesion force than the linear pillars. Linear fitting of the data points gives a slope of 1.39 ± 0.08 (R^2 of 0.98) and 0.55 ± 0.04 (dimensionless) (R^2 of 0.96) for branched pillars and linear pillars, respectively. These slopes denote the effectiveness of shear adhesion force of the two samples against the smooth glass surface. This translates to the branched pillars outperforming the linear pillars in shear adhesion measurements by 150% or 2.5 times (for the same pillars' height and base pillars' diameter (refer to Figure S1)).

Figure 4b shows the estimated area of residual deformation of the test substrates obtained from image analysis for different preloads. Except at the very low preload, higher area of residual deformation between the branched pillars and the glass surface was recorded as compared to the linear pillars. As previously explained, this higher area of residual deformation of the branched pillars provides an explanation for the higher effective shear adhesion force of the branched pillars as compared to that of the linear pillars as shown in Figure 4a. At the very low preload

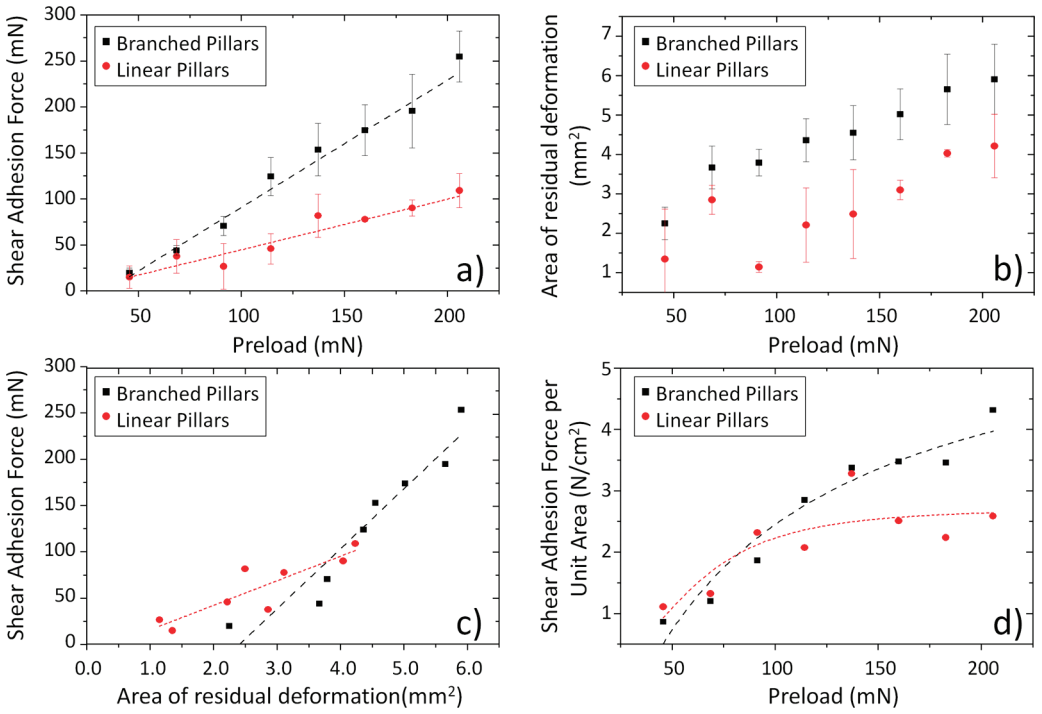

Figure 4. (a) Shear adhesion force *versus* preload for branched and linear pillars. Linear fitted slopes of 1.39 ± 0.08 (R^2 of 0.98) and 0.55 ± 0.04 (R^2 of 0.96) for branched pillars and linear pillars, respectively. (b) Area of residual deformation (effective contact area after preload removal) of pillars against glass slide *versus* preload. (c) Shear adhesion force of both branched and linear pillars with respect to its area of residual deformation. Linear fitted slopes for branched and linear pillars are 65.2 ± 8.2 mN/mm² (R^2 of 0.90) and 26.6 ± 5.6 mN/mm² (R^2 of 0.75), respectively. (d) Shear adhesion force per unit effective contact area of these two types of pillars *versus* preload. Error bar indicates one standard deviation.

region in Figure 4b, there is no significant difference in the area of residual deformation between the branched and linear pillars. Thus, consequently at these low preloads, the shear adhesion force as shown in Figure 4a registered similar values for both the branched and linear pillars substrates. This finding confirms the role that contact area plays in shear adhesion.

Our studies indicating that the adhesion force of a branched pillar topography is superior to that of a linear pillar topography could be explained using the classical beam theory.[27] According to the theory, the deformation of a beam may be described by

$$M = EI\kappa \quad (1)$$

where M is the applied bending moment, κ is the curvature, E is the Young's modulus, and I is the moment of inertia of the beam's cross section. Collectively, EI is referred as the flexural rigidity of the beam, and it dictates the ease of deformation of the beam. The smaller the value of EI, the more flexible is the beam. For two different beams of the same material, E will be the same, and their flexibility will be inversely proportional to their moment of inertia I.

I for a circular cross section is $\pi D^4/64$,[28] where D is the diameter of the linear pillar (see Figure S5a in the Supporting Information). The diameter at the top of the branched pillar, d, is ~1/3 of the diameter of the linear pillar, D. Therefore, the I at the top of a single branched pillar is $1/3^4(\pi D^4/64)$, which is significantly (81 times) less than that of a linear pillar. There are four branched pillars for every single linear pillar. Due to dissimilar planes, only two out of four of the branched pillars are assumed to act in unison as shown in Figure S5b (see Supporting Information), the effective moment of inertia will be $2/3^4(\pi D^4/64)$, which is 40 times less than that of the single linear pillar. Hence, the branched pillar configuration is significantly more flexible than the linear pillar configuration. This increase in flexibility gives rise to an increase in effective area in contact (through side contact)[26] to a test surface (see Figure S5c,d in the Supporting Information).

To further substantiate the explanation, the SEM images in Figure 5a,b were taken for linear pillars and branched pillars, respectively, after the same shear adhesion test was performed. The images clearly show that there are more branched pillars bent in the direction of shear, thus indicating higher indicative contact area with the glass surface.

The relationship between shear adhesion force and area of residual deformation for both branched and linear pillars is analyzed in Figure 4c. The linear fitted slopes for branched and linear pillars are 65.2 ± 8.2 and 26.6 ± 5.6 mN/mm², respectively. The physical meaning of the values is, for every unit of increased area,

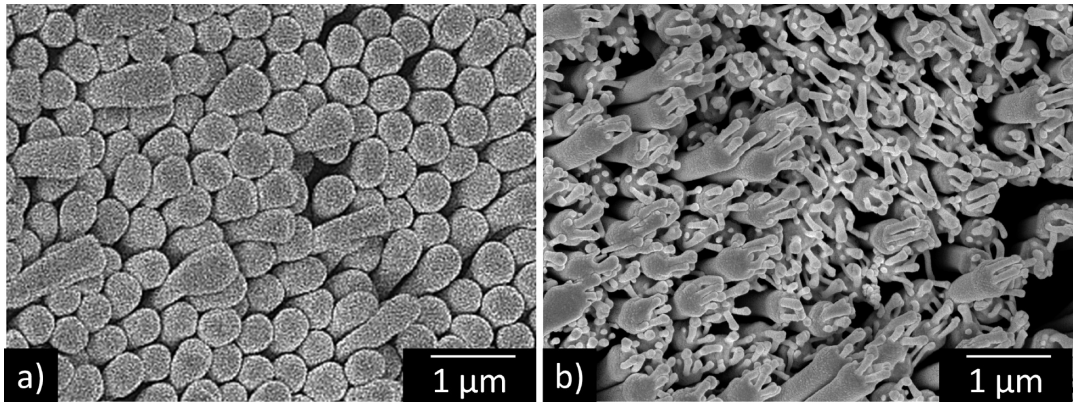

Figure 5. SEM images of samples after shear adhesive tests were performed for (a) linear pillars and (b) branched pillars. More branched pillars bent in the direction of shear indicating more area of contact.

there is an increase of 65.2 and 26.6 mN of shear adhesion force for branched and linear pillars, respectively. Branched pillars show a higher increase of shear adhesion force with a smaller increase in area of residual deformation as compared to the linear pillars. This is most likely due to the top pillars of the branched pillars being able to reach into the finer asperities of the glass surface reaching an atomic gap of 0.3 nm.[7] Consequently, there is an increase of van der Waals attraction between the surfaces. These results are in fact in agreement with the general equation for shear adhesion force (friction force) of two sliding surfaces (of molecular smoothness)[29] given by

$$F_{Sad} = \mu L + S_c A_{eff} \quad (2)$$

where μ is the coefficient of friction of pristine polycarbonate on glass surface, L is the preload normal to sliding, A_{eff} is the effective contact area, and S_c is the shear strength accounting for the intermolecular adhesive force also known as van der Waals force.[30] S_c itself is a function of $\Delta\gamma$ which is the adhesion energy hysteresis (materials dependent) and δ ($\approx$0.3 nm)[7] which is the atomic gap between the surface and the fibril for effective van der Waals attraction (eq 3).

$$S_c = \varepsilon\Delta\gamma/\delta \quad (3)$$

The term μL in eq 2 denotes load-controlled friction and $S_c A_{eff}$ denotes adhesion-controlled friction.[31] This equation shows that the shear adhesion force F_{Sad} is a function of both normal load and effective contact area, and that an increase in effective contact area will result in an increase in shear adhesion force.

It may be debatable that eq 2 is not well represented by Figure 4b, as the effective contact area may be induced by the externally applied normal load as discussed by Gao *et al.*[31] However, the results in Figure 3a, showing increasing adhesion force for the same preload for repeated tests, indicate that the effective contact area is not only a function of the preload but also the actual structural state of the pillars, which is reflected by the residual deformation.

Figure 4d is derived from the calculated shear adhesion force per unit area of residual deformation of the two types of pillars plotted against its respective preloads. It shows that both the branched and linear pillars initially show similar values of shear adhesion force per unit area, but the difference increases as the preloads are increased, indicating that the branched pillars have superior adhesive performance. In addition, it also shows that, for linear pillars, shear adhesion force per unit area approached saturation for a preload of 90 mN. In contrast, for branched pillars, although the rate of increase of shear adhesion force per unit area decreased with an increase in preload, it did not reach saturation for the maximum preload investigated. This could be understood from the perspective of collective stiffness of the linear and branched pillars. The collective stiffness of the linear pillars seemingly reached its maximum. This is equivalent to a compact film and, as such, no amount of increase in preload would increase the shear adhesion strength. However, the collective stiffness of the branched pillars is lower than the linear pillars, which is the reason why the adhesion strength of the branched pillars has yet to reach saturation.

It is worth noting that the area of residual deformation for both the linear and branched pillars was initially 1−3 mm^2 and gradually increased to 3.5−5 mm^2 for linear pillars and 5−7 mm^2 for branched pillars after applying a preload of 210 mN. Given that the size of the samples tested were 1×1 cm^2, the area of residual deformation corresponding to the area that had been in contact could only reach 7% of the total sample area. The reason for this low value is the low compliance and unevenness of the thick and rigid polymer backing film of $\sim$150 μm in thickness, which prevented some of the topographic structures from reaching the test surface. Hence having a thick backing layer is detrimental in dry adhesion tests. Previous authors have resolved this issue by fabricating adhesive structures on thin and flexible substrates.[11]

Nonetheless, it can be seen from Table 1 that the shear adhesion force of the hierarchical structures

TABLE 1. Comparisons of Normal and Shear Adhesion Forces of the Natural Gecko Foot Hair and the Fabricated Hierarchical Structures As Reported

material type	material (modulus)	feature size	type of measurement	normal adhesion force	shear adhesion force	reference
hard	β-keratin	micro & nano	macroscopic	1	10 N/cm^2	7
	PMMA (2.4 GPa)	micro & nano		not available		15
	PC (2 GPa)	nano	macroscopic	not available	6.5 N/cm^2	this work
soft	PDMS (1.8 MPa)	micro	microscopic	~4 N/m^2	not available	16
	PU (3 MPa)	micro	microscopic	~5.3 kN/m^2	not available	17
	PUA (19.8 MPa)	micro	macroscopic	not available	9 N/cm^2	18

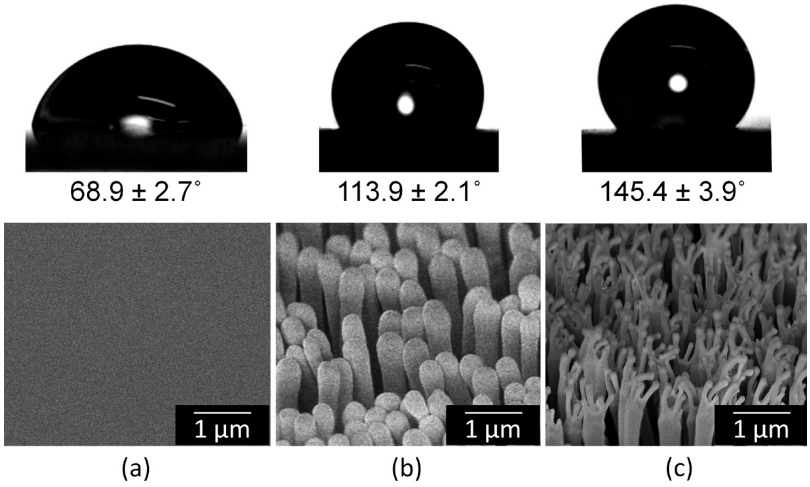

Figure 6. Water contact angles and corresponding images of the topography for (a) pristine polycarbonate, (b) linear polycarbonate pillar structure, and (c) branched polycarbonate pillar structure.

produced in this work reached a value of 6.5 N/cm^2, which is 35% less in force than the shear adhesion force of the natural gecko foot hair (β-keratin) (10 N/cm^2).[7] This could be due to the synergy of micro- and nanoscale features of the natural gecko foot hair when used in unison as optimized by nature. Table 1 also shows the comparison of hierarchically structured tapes fabricated in this work with those reported by other authors. However, direct comparisons of shear adhesion performance of the various reported synthetic gecko-inspired adhesives are difficult as there are variations in terms of the type of polymeric materials used, the range of feature sizes as well as the type of measurements conducted.

Another characteristic of highly dense topographical structures is to change the wetting properties of a surface. Kustandi *et al.*[15] and Jeong *et al.*[32] have reported a marked increase on the contact angles of water as the hierarchy of the topography on a surface is increased. This phenomenon was also observed for the branched pillar topography fabricated in this work. The water contact angle on a pristine PC surface was measured to be 68.9 ± 2.7°, which increased to 113.9 ± 2.1° for linear pillars and 145.4 ± 3.9°for branched pillars. Figure 6 shows the images of water contact angles on pristine PC, linear pillar, and branched pillar topographical substrates. Such increase in hydrophobicity is important for the use of the hierarchically branched pillar topography in gecko-like adhesive applications for good self-cleaning ability, especially for repeated usage as dry adhesive tapes.

CONCLUSION

We have successfully fabricated a gecko inspired hierarchical structure on a stiff polymer by nanoimprinting technique using specifically prepared multitiered branched porous anodic alumina templates. We have shown that the hierarchical structure improves the shear adhesion force over the corresponding linear structure by 150%. It was determined that the effective stiffness of the hierarchical branched structure is lower than that of the linear structure. This allows for a more efficient bending of the branched topography and a better compliance to a test surface hence resulting in larger number of contacts, i.e., larger contact area of dry adhesive films with a hierarchical topography and as a result, a larger shear adhesion force. The hierarchically branched pillar structures also showed a marked increased in hydrophobicity which is a salient property required in practical applications of dry adhesives. Future work entails reducing the rigidity and thickness of the backing layer of the adhesive substrate to facilitate the conformal contact to various surfaces hence improving the

adhesive force of dry adhesive tapes. Investigation is planned on a third tier comprising of microscale pillars to better mimic the natural gecko foot hairs for higher shear adhesion. It is envisaged that such understanding will lead to optimal design and fabrication of dry adhesives.

EXPERIMENTAL DETAILS

Template Fabrication. Commercially available aluminum sheets (Goodfellow 99.999%, 0.25 mm thick) were cut to size, typically 20 mm × 30 mm. The sample was then electropolished in a 1:4 mixture of 60% perchloric acid and ethanol at the following conditions: constant potential of 25 V; temperature of 5 °C; time of 4 min. The sample was mounted onto a glass slide, and the edges were insulated (with Elmer's E949 Squeez 'N Caulk 6-Ounce, Clear) to prevent excess charge formation at the edges thus avoiding non-homogeneous anodization across the substrate. The sample was subsequently immersed into a thermally insulated anodization bath containing the electrolyte, with the bath placed on a cold plate to maintain constant temperature. A platinum mesh acting as a counter electrode was then immersed into the electrolyte. The positive and negative terminals of a power supply were connected to the aluminum sample and platinum mesh, respectively. Long anodization was carried out using 0.3 M H_3PO_4 at constant voltage of 130 V at 2 °C for 7 h. The alumina layer obtained was then etched with a mixture of 45 g/L chromic(VI) oxide and 3.5 vol % phosphoric acid at 55 °C for 30 min. The sample was then rinsed and dried before the second anodization step under the same conditions for 5 min. The first tier was obtained by anodizing with 0.3 M H_3PO_4 at a constant potential of 130 V at room temperature for 4 h followed by pore widening in 5 wt % H_3PO_4 for 120 min. The second tier anodization was performed at 80−100 V using 0.15 M $C_2H_2O_4$ acid at 0 °C. The current stabilized almost immediately at around 1 mA (from a high current on turning on the power supply). Subsequent increase in current signaled the generation of the second tier of the PAA template, and the process was then timed for 4 min. Subsequently, pore widening was performed for 90 min with the same barrier layer thinning solution (5 wt % H_3PO_4) at the same conditions.

Polymer Nanostructure Replication by Nanoimprinting. The fabricated PAA template (1 × 1 cm^2) was placed on top of a commercial 250 μm thick polycarbonate (PC) film. This assembly was loaded into an Obducat Nanoimprinter System (NIL 4″). The temperature was raised to 175 °C (25 °C above T_g), and a pressure of 15 bar was applied for 20 min under vacuum. The assembly was then cooled to room temperature, and demolding of the polymeric structures was performed by peeling off the PAA template.

Qualitative Shear Adhesion Force Measurements. The sample was cut into 1 × 1 cm^2 size. The back of the sample was glued using superglue (cyanoacrylate adhesive) to a metallic disk (weighing 1.41 g and 16.26 mm in diameter and 1.02 mm in thickness). The sample was then placed with the pillars facing against a cleaned glass slide. With one end of the glass slide fixed acting as a pivot, the other end was raised. The angle at which the coin started to slide was measured.

Quantitative Shear Adhesion Force Measurements. Shear adhesion tests were performed at room temperature (~22 °C) and humidity of ~70%. The shear adhesion measurements were conducted using an Instron 5543 single column universal testing machine. A 2.5 N load cell was fixed to the machine's crosshead. To translate vertical movement to lateral movement for the shear tests, a ball-bearing Teflon pulley aligned directly under the load cell was used. A thin copper wire of 30 μm was employed to connect the load cell to the test sample. A sample (1 × 1 cm^2) was then placed with the pillars facing a glass slide. Teflon-taped side guides each with 0.5 mm clearance were fixed onto the glass slide on both sides of the sample to prevent the sample from twisting during pulling when conducting the shear test. As preload, a dead weight (45 mN) was superglued on top of the sample, and then the copper wire was pulled to just taut. The shear force was registered as the sample was sliding on the glass surface when the crosshead was extended upward. The sample was pulled at a constant speed of 5 cm/min with a total displacement of 5 cm. After each measurement, the preload was removed and the sample was observed under a microscope where images of the contact area (at zero preload) were captured. The sample was then returned to be tested with increased preloads. Preloads were increased in stepped increments of 25 mN, and the same procedure was repeated for each increment. Each test was repeated with three samples. Figure S4a,b (see Supporting Information) illustrates the schematic as well as the actual test setup, respectively.

Estimation of the Area of Residual Deformation. For each sample, a control image was first captured prior to the shear test using an optical microscope. As there is limitation by the field of view of the microscope in capturing the entire area of the sample, images were taken in parts and were stitched together before analyzing with an image processing software (ImageJ, version 1.41o). The stitched image was originally in RGB color and was subsequently quantized to 8-bit grayscale. On the basis of the percentage of pixels of the light contrast of the grayscale image, the area fraction of the control image was determined. This was used as a benchmark for all subsequent images. The same procedure was applied after each shear force measurement and after the removal of the preload. The area of residual deformation (effective contact area at zero preload) was then estimated by subtracting the area fraction of each image after each shear force measurement from the control image.

Acknowledgment. The authors gratefully acknowledge Mr. Augustine Cheong for the mechanical testing setup. This research has been supported by the Agency for Science Technology and Research (A*STAR): Institute of Materials Research & Engineering.

Supporting Information Available: Figures S1−S5. This material is available free of charge *via* the Internet at http://pubs.acs.org.

REFERENCES AND NOTES

1. Irschick, D. J.; Austin, C. C.; Petren, K.; Fisher, R. N.; Losos, J. B.; Ellers, O. A Comparative Analysis of Clinging Ability Among Pad-Bearing Lizards. *Biol. J. Linnean Soc.* **1996** *59*, 21–35.
2. Santos, D.; Spenko, M.; Parness, A.; Kim, S.; Cutkosky, M. Directional Adhesion for Climbing: Theoretical and Practical Considerations. *J. Adhes. Sci. Technol.* **2007,** *21*, 1317–1341.
3. Zhao, B.; Pesika, N.; Rosenberg, K.; Tian, Y.; Zeng, H.; McGuiggan, P.; Autumn, K.; Israelachvili, J. Adhesion and Friction Force Coupling of Gecko Setal Arrays: Implications for Structured Adhesive Surfaces. *Langmuir* **2008,** *24*, 1517–1524.
4. Autumn, K.; Peattie, A. M. Mechanisms of Adhesion in Geckos. *Integr. Comp. Biol.* **2002,** *42*, 1081–1090.
5. Rodolfo, R.; Ernst, V. The Structure of the Digital Setae of Lizards. *J. Morphol.* **1965,** *117*, 271–293.
6. Persson, B. N. J.; Gorb, S. The Effect of Surface Roughness on the Adhesion of Elastic Plates with Application to Biological Systems. *J. Chem. Phys.* **2003,** *119*, 11437.
7. Autumn, K.; Liang, Y. A.; Hsieh, S. T.; Zesch, W.; Chan, W. P.; Kenny, T. W.; Fearing, R.; Full, R. J. Adhesive Force of a Single Gecko Foot-Hair. *Nature* **2000,** *405*, 681–685.
8. Arzt, E.; Gorb, S.; Spolenak, R. From Micro to Nano Contacts in Biological Attachment Devices. *Proc. Natl. Acad. Sci. U.S.A.* **2003,** *100*, 10603–10606.
9. Bhushan, B.; Peressadko, A. G.; Kim, T.-W. Adhesion Analysis of Two-Level Hierarchical Morphology in Natural

Attachment Systems for `Smart Adhesion'. *J. Adhes. Sci. Technol.* **2006,** *20*, 1475–1491.
10. Sitti, M.; Fearing, R. S. Synthetic Gecko Foot-Hair Micro/Nano-Structures as Dry Adhesives. *J. Adhes. Sci. Technol.* **2003,** *17*, 1055–1073.
11. Geim, A. K.; Dubonos, S. V.; Grigorieva, I. V.; Novoselov, K. S.; Zhukov, A. A.; Shapoval, S. Y. Microfabricated Adhesive Mimicking Gecko Foot-Hair. *Nat. Mater.* **2003,** *2*, 461–463.
12. Gao, H. J.; Wang, X.; Yao, H. M.; Gorb, S.; Arzt, E. Mechanics of Hierarchical Adhesion Structures of Geckos. *Mech. Mater.* **2005,** *37*, 275–285.
13. Kim, T. W.; Bhushan, B. Adhesion Analysis of Multi-Level Hierarchical Attachment System Contacting with a Rough Surface. *J. Adhes. Sci. Technol.* **2007,** *21*, 1–20.
14. Kim, T. W.; Bhushan, B. Effect of Stiffness of Multi-Level Hierarchical Attachment System on Adhesion Enhancement. *Ultramicroscopy* **2007,** *107*, 902.
15. Kustandi, T. S.; Samper, V. D.; Ng, W. S.; Chong, A. S.; Gao, H. Fabrication of a Gecko-Like Hierarchical Fibril Array Using a Bonded Porous Alumina Template. *J. Micromech. Microeng.* **2007,** *17*, N75–N81.
16. Greiner, C.; Arzt, E.; del Campo, A. Hierarchical Gecko-Like Adhesives. *Adv. Mater.* **2009,** *21*, 479–482.
17. Murphy, M. P.; Kim, S.; Sitti, M. Enhanced Adhesion by Gecko-Inspired Hierarchical Fibrillar Adhesives. *ACS Appl. Mater. Interfaces* **2009,** *1*, 849–855.
18. Jeong, H. E.; Lee, J.-K.; Kim, H. N.; Moon, S. H.; Suh, K. Y. A Nontransferring Dry Adhesive with Hierarchical Polymer Nanohairs. *Proc. Natl. Acad. Sci. U.S.A.* **2009,** *106*, 5639–5644.
19. Autumn, K. *Properties, Principles and Parameters of the Gecko Adhesive System*; Springer-Verlag: Berlin, 2006; pp 225−255.
20. Ho, A. Y. Y.; Gao, H.; Lam, Y. C.; Rodríguez, I. Controlled Fabrication of Multi-Tiered Three-Dimensional Nanostructures in Porous Alumina. *Adv. Funct. Mater.* **2008,** *18*, 2057–2063.
21. Suh, K. Y.; Kim, Y. S.; Lee, H. H. Capillary Force Lithography. *Adv. Mater.* **2001,** *13*, 1386–1389.
22. Keller, F.; Hunter, M. S. A.; Robinson, D. L. Structural Features of Oxide Coatings on Aluminum. *J. Electrochem. Soc.* **1953,** *100*, 411–419.
23. Lee, J.; Majidi, C.; Schubert, B.; Fearing, R. Sliding-Induced Adhesion of Stiff Polymer Microfibre Arrays. I. Macroscale Behaviour. *J. R. Soc. Interface* **2008,** *5*, 835.
24. Peressadko, A.; Gorb, S. N. When Less Is More: Experimental Evidence for Tenacity Enhancement by Division of Contact Area. *J. Adhes.* **2004,** *80*, 247–261.
25. Varenberg, M.; Peressadko, A.; Gorb, S.; Arzt, E. Effect of Real Contact Geometry on Adhesion. *Appl. Phys. Lett.* **2006,** *89*, 121905.
26. Majidi, C. S.; Groff, R. E.; Fearing, R. S. Attachment of Fiber Array Adhesive through Side Contact. *J. Appl. Phys.* **2005,** *98*, 103521-5.
27. Gere, J. M.; Timoshenko, S. P. *Mechanics of Materials*; Cengage Learning: Toronto, Canada, 1997.
28. Chen, B.; Wu, P. D.; Gao, H. Hierarchical Modelling of Attachment and Detachment Mechanisms of Gecko Toe Adhesion. *Proc. R. Soc. London, Ser. A* **2008,** *464*, 1639.
29. Zeng, H.; Pesika, N.; Tian, Y.; Zhao, B.; Chen, Y.; Tirrell, M.; Turner, K. L.; Israelachivili, J. Frictional Adhesion of Patterned Surfaces and Implications for Gecko and Biomimetic Systems. *Langmuir* **2009,** *25*, 7486.
30. Homola, A. M.; Israelachivili, J. N.; Mcguiggan, P. M.; Gee, M. L. Fundamental Experimental Studies in Tribology: The Transition from "Interfacial" Friction of Undamaged Molecularly Smooth Surfaces to "Normal" Friction with Wear. *Wear* **1990,** *136*, 65.
31. Gao, J.; Luedtke, W. D.; Gourdon, D.; Ruths, M.; Israelachvili, J. N.; Landman, U. Frictional Forces and Amontons' Law: From the Molecular to the Macroscopic Scale. *J. Phys. Chem. B* **2004,** *108*, 3410–3425.
32. Jeong, H. E.; Lee, S. H.; Kim, J. K.; Suh, K. Y. Nanoengineered Multiscale Hierarchical Structures with Tailored Wetting Properties. *Langmuir* **2006,** *22*, 1640–1645.